Available online at www.sciencedirect.com

ScienceDirect

journal homepage: www.elsevier.com/locate/he

Steam reforming of acetic acid in the presence of Ni coated with SiO_2 microsphere catalysts

Sahika Ozel [a], *Gamze Gündüz Meric* [b], *Huseyin Arbag* [a], *Levent Degirmenci* [b,*], *Nuray Oktar* [a]

[a] *Department of Chemical Engineering, Gazi University, 06570, Ankara, Turkey*
[b] *Chemical Engineering Department, Bilecik Seyh Edebali University, Gulumbe Campus, Bilecik, Turkey*

HIGHLIGHTS

- The highest activity was obtained with Ni loadings between 5-10%..
- The effect of H_2O/AcOH ratio on hydrogen selectivity was statistically irrelevant.
- The opposite trend between CO_2 and CO selectivities was due to RWGS.
- The affinity through decarboxylation reaction was limited.
- Carbon deposited through ketonazation and aldol-condensation reactions.

GRAPHICAL ABSTRACT

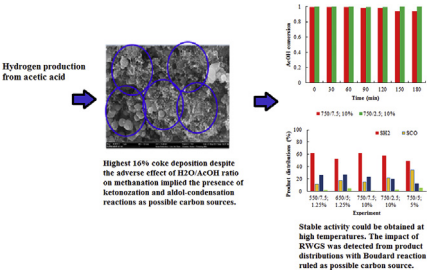

ARTICLE INFO

Article history:
Received 16 March 2020
Received in revised form
13 May 2020
Accepted 15 May 2020
Available online 19 June 2020

Keywords:
Steam reforming
Acetic acid
Boudouard
Methanation
Ketonozation
Aldol-condensation

ABSTRACT

Steam reforming of acetic acid was investigated in the presence of Ni@SiO_2 microsphere catalysts. The effects of Ni loading, H_2O/AcOH ratio, and temperature on hydrogen selectivity and acetic acid conversion were determined via statistical analysis. Results indicated the dependence of parameters on hydrogen selectivity.

The stable activity observed for the reaction conducted at 2.5H_2O/AcOH ratio and 750 °C implied future utilization potential of the catalyst for time on stream experiments despite the inevitable coke formation. Boudard reaction and methane decomposition, known as possible carbon sources, was ruled out due to the opposite trends between CO_2 and CO selectivities and mitigation of methanation reactions. The ambiguous pattern of conversions observed for varying H_2O/AcOH implied the presence of a different reaction path leading to consecutive ketonozation of acetic acid and aldol-condensation of acetone as the primary sources of carbon deposition.

* *Corresponding author.*
E-mail address: levent.degirmenci@bilecik.edu.tr (L. Degirmenci).
https://doi.org/10.1016/j.ijhydene.2020.05.146

Introduction

Global energy demand is continually increasing due to the conjugate increase in population and quality of life. Fossil fuels, the primary source in meeting this energy demand, will probably be inadequate to keep up due to reduced availability associated with its nonhomogeneous distribution [1–3].

Hydrogen is among the best candidates as a replacement to fossil fuels. Hydrogen can be produced from biomass-derived products by an environmentally benign process, which results in the formation of water [3].

Hydrogen production is achieved through two routes, which include the utilization of syngas or bio-oil in reforming reactions. Bio-oil is a complex structure, and its use as a feedstock accompanies several problems. Side product formation, coke accumulation, rapid catalytic deactivation are common problems encountered in the case of bio-oil utilization. Acetic acid is among the ingredients of bio-oil with the amounts of 5–10%, which is a significant amount for one compound and a promising alternative for use in steam reforming reactions [4–6].

Substituting bio-oil with a single compound is the first step in solving the problems encountered in reactions. In other words, coke formation and resulting catalytic deactivation are still two major obstacles for the commercialization of the process. Steam reforming reactions are conducted in the presence of catalysts with the use of different active metals: Ni, Co, Mg, Pd, Rh, Fe, and supports: SiO_2, Al_2O_3, La_2O_3 and halloysides [7–12].

Ni-based catalysts are more efficient and preferable for use in hydrogen production due to ease of modification and low cost [13,14]. However, Ni-based catalysts are inadequate in preventing coke formation despite their high C–C cleavage activity, and some modifications need to be conducted in order to increase their efficiencies. The addition of alkali or alkaline-earth metals such as K, Mg, Ca, Ba, etc., rare earth metals (La, Ce, etc.) and boron nitride as the second active component were recently conducted and accomplished approaches. These metals can suppress coke formation because of their excellent oxygen storage capacity [15–22].

Coating metal particles in porous silica-based shell materials are the latest approach in preventing deactivation of the catalyst via sintering and coke formation [23,24]. These core-shell structures show excellent catalytic performance in the reforming reactions [25,26] and also exhibits excellent stability during long-term durability tests [27]. Porous silica shell provides an efficient and homogenous distribution of the metal in the structure. Strong interaction between the metal and silica core enables the formation of a physical barrier, and this confinement effect provides excellent resistance to sintering at high temperatures [28,29]. Ni and bimetallic Ni–Co based core-shell microsphere catalysts ($Ni@SiO_2$, $NiCo@SiO_2$, $Ni@SiO_2$, $Co@SiO_2$) were recently investigated in the dry reforming of methane, in our previous studies [30–32]. These catalysts indicated high activities. Coke suppression was the highlight of these microsphere catalysts, which was achieved by SiC formation. This SiC formation was introduced as a situation unique to microsphere structure [30–32]. Suppression of coke in the presence of a hydrocarbon could also be valid for the steam reforming of acetic acid. Resistance to sintering at high temperatures also increases the possibility of these catalysts' utilization.

Acetic acid (AcOH) is a simple organic compound, but steam reforming of AcOH involves a complex reaction network [13,33]. The overall reaction is presented by Eq. (1).

$$CH_3COOH + 2_{H2}O \rightarrow 2_{CO2} + 4_{H2} \qquad \Delta H^{\circ}: 131.4\,kJ/mol\,(298\,K) \quad (1)$$

Hydrogen is produced from AcOH by thermal decomposition (Eq. (2)) and water gas shift reactions (Eq. (3)).

$$CH_3COOH \leftrightarrow 2_{H2} + 2CO \qquad \Delta H^{\circ}: 213.4\,kJ/mol\,(298\,K) \quad (2)$$

$$CO + H_2O \leftrightarrow H_2 + CO_2 \qquad \Delta H^{\circ}: -41\,kJ/mol\,(298\,K) \quad (3)$$

Due to the complexity of the steam reforming of AcOH, many side reactions affect the product distribution. Acetic acid could degrade through decarboxylation reaction (Eq. (4)) and the formation of acetone (Eq. (5)) during the steam reforming reaction. Coke formation during steam reforming of AcOH leads to catalyst deactivation. Coke is mainly produced by Boudouard (Eq. (6)) and methane cracking (Eq. (7)) side reactions.

$$CH_3COOH \leftrightarrow CH_4 + CO_2 \qquad \Delta H^{\circ}: -33.5\,kJ/mol\,(298\,K) \quad (4)$$

$$2CH_3COOH \rightarrow (CH_3)_2CO + CO_2 + H_2O \qquad \Delta H^{\circ}: 38\,kJ/mol\,(298\,K) \quad (5)$$

$$2CO \leftrightarrow C + CO_2 \qquad \Delta H^{\circ}: -172.4\,kJ/mol\,(298\,K) \quad (6)$$

$$CH_4 \leftrightarrow C + 2_{H2} \qquad \Delta H^{\circ}: 74.8\,kJ/mol\,(298\,K) \quad (7)$$

Based on the literature survey, metal-containing core-shell catalysts in general and core-shell microspheres, in particular, were determined as exceptional candidates for use in steam reforming of acetic acid. In this context, the present study was conducted to evaluate the performance of Ni-based microsphere catalysts in variant acetic acid/H_2O ratio, Ni loading amount and reaction temperature values for the steam reforming of acetic acid. Response surface methodology, a versatile statistical approach, was adopted for experimental design. This methodology was particularly useful in decreasing the number of experimental runs, which was 18 in our study, including five replicates. One-way variance analysis (ANOVA) was conducted to statistically determine the effect of parameters on acetic acid conversion and hydrogen selectivity values. The threshold of parameter significance was selected as $p < 0.05$. X-ray diffraction (XRD), thermogravimetric analysis (TGA), scanning electron microscopy (SEM), and Raman spectroscopy were applied to the catalysts obtained after the reaction with intent to clarify the effect of coke formation on catalyst structure.

Experimental

Preparation of Ni core-shell micro-spheres

Ni core-shell microspheres are prepared by a modified sol-gel microencapsulation method [30,31]. The theoretical loading

amount of Ni inside the catalyst was selected as 1.25, 5 and 10% of total silicium weight. Initial steps in synthesis were preparation of water and oil phases. Water phase consisted of $Ni(NO_3)_26H_2O$ (Merck) and the surfactant hexadecyltrimethylammonium bromide (CTAB) which were dispersed in 20 mL of deionized water by ultrasonication (15 min). Subsequently, a mixture of 50 mL ethanol and 10 mL 25 wt % ammonia solution (oil phase) was prepared, in which the water phase was added, and the resulting solution was homogenized at 5000 rpm (5 min). 5 mL of TEOS (tetraethylorthosilicate) was added dropwise to this solution, and the suspension was stirred at room temperature for 6 h. The powder was obtained following a sequential washing (ethanol and deionized water, 3 times) and drying (room temperature, 24 h) procedures, and the catalyst was calcined at 750 °C for 6 h. The catalyst was named as $Ni@SiO_2$ to maintain easy follow-up.

Catalytic activity tests of $Ni@SiO_2$ catalysts

Catalytic activity tests were performed in a fixed bed tubular flow reactor (6 mm inner diameter of the quartz reactor tube) with 0.1 g of catalyst loading in the center. The catalyst was stabilized with quartz wool placed in both ends of the reactor. The catalyst was reduced at 750 °C in a flow of H_2 (3 h) to obtain Ni containing particles. The duration of reaction and reduction was kept 3 h at all times. The temperature was altered as 550, 650, 750 °C, and the reaction was conducted under atmospheric pressure. Water and acetic acid were continuously fed with molar ratios of $AcOH/H_2O = 1/2.5,1/5,1/7.5$. Reactants were transferred to the reactor with a total vapor phase flow rate of 82.5 mL/min. Gas products were analyzed with a gas chromatograph (GC) (Agilent Model 6890N) equipped with a Porapak-S column. Liquid products were also quantified by the same GC in 1-h intervals. A condenser was placed between the reactor and GC to remove water and possible unreacted acetic acid. Analyses of liquid products indicated negligible amounts of acetic acid along with water.

The conversion of acetic acid (X_{AcOH}) (Eq. (8)), the selectivity of products (S_P) (Eq. (9)) and H_2 (S_{H2}) (Eq. (10)) were calculated according to the equations below [34,35];

Statistical analyses

Reaction parameters investigated in experiments and experimental design were given in Supplementary File (Tables 1 and 2). Parameters were coded as −1, 0, and 1, with −1 being the lowest and 1 being the highest value. Statistical analysis was conducted on X_{AcOH} and S_{H2} values. Multiple regression analysis was applied to produce second-order interaction coefficients. Model coefficients and analyses of variance were evaluated to determine the fit of the proposed model according to the equation below:

$$Y_c \text{ and } Y_L = \beta_0 \sum_{i=1}^{k} \beta_{ij} X_i + \sum_{i=1}^{k} \beta_{ij} X_i^2 + \sum_{i,i>j}^{k} \sum_{j}^{k} \beta_{ij}\beta_{ij} X_i X_j$$

Y is designated for the responses (Y_c for X_{AcOH} and Y_L for S_{H2}, respectively), and i and j were given for linear and quadratic coefficient. β and k were assigned to the regression coefficient and the number of factors, respectively.

Coke formation and characterization of spent $Ni@SiO_2$ catalysts

Characterization of fresh $Ni@SiO_2$ catalysts was recently conducted with Nitrogen adsorption-desorption, X-ray diffraction (XRD), Scanning electron microscopy (SEM) and inductively coupled plasma-mass spectroscopy (ICP-MS) techniques. Results were elaborated in our previous studies [30].

Characterization analyses were performed on selected catalysts recovered after 3 h of reaction. X-ray diffraction (XRD) analysis with a Panalytical Empyrean instrument at 200 kV and 50 mA with 2Θ values ranging between 5 and 80° and with a speed of 10°/min. Scanning electron microscopy (SEM) was carried out with a Quanta 400F Field Emission SEM device to visualize carbon formation and to determine possible changes in surface morphologies. PerkinElmer Pyris1 instrument was utilized for thermogravimetric analysis (TGA). Analyses were performed in the presence of airflow, in a temperature range of 25–900 °C and at a heating rate of 10 °C/min. Raman spectroscopy was employed to detect carbon formation. Analyses were performed in a Bruker FRA 106/S device equipped with a 532 nm laser.

$$X_{AcOH} = \frac{\textit{inlet molar flow rate of AcOH} - \textit{outlet molar flow rate of AcOH}}{\textit{inlet molar flow rate of AcOH}} \tag{8}$$

$$S_P = \left(\frac{\textit{moles of product}}{2(\textit{inlet molar flow rate of AcOH} - \textit{outlet molar flow rate of AcOH})}\right)100 \tag{9}$$

$$S_{H2} = \left(\frac{\textit{moles H2 produced}}{4(\textit{moles AcOH reacted})}\right)100$$

$$\left(\text{moles AcOH reacted} = \frac{(\textit{moles of CH4} + \textit{CO2} + \textit{CO in the product stream})}{2}\right) \tag{10}$$

Table 1 – Results obtained from reaction experiments.

% Ni loading amount	Experimental conditions[a]	X_{AcOH} (%)	S_{H2} (%)
1.25	550/2.5	23	58.0
1.25	550/7.5	40	61.5
1.25	650/5.0	81	57.7
1.25[b]	750/2.5	83.0	52.5
1.25	750/7.5	55.0	44.6
5	550/5.0	27.0	61.5
5	650/2.5	28.0	57.3
5	650/5.0	97.0	59.1
5	650/5.0	95.0	58.9
5	650/5.0	95.0	58.8
5	650/5.0	95.0	58.6
5	650/7.5	51.0	55.8
5[b]	750/5.0	59.0	53.4
10	550/2.5	45.0	60.6
10	550/7.5	41.0	64.3
10	650/5.0	45.0	60.3
10[b]	750/2.5	100	57.3
10	750/7.5	94.0	61.5

[a] Experimental conditions: Temperature (°C)/H_2O/AcOH ratio, respectively. All experiments were conducted for 3 h in the presence of a 0.1 g catalyst.
[b] These catalysts were recovered from the reactor and further used in characterization analyses (See section Coke formation and characterization of spent Ni@SiO2 catalysts).

Results and discussions

Catalytic activity tests of Ni@SiO_2 catalysts/statistical analyses

Ni crystals are prone to form carbon filaments, which result in the breakdown of the particle from the support structure. Hence encapsulation of Ni inside the microsphere structure was the first and one of the most crucial steps in increasing catalyst lifetime in reactions [36]. Characterization analyses of fresh catalysts in the present study revealed the formation of mesoporous microspheres with narrow pore size distributions and Ni particles situated mainly on the near-surface layer [30]. Coating Ni with SiO_2 was the first step in decreasing carbon formation during the steam reforming of acetic acid.

Our research group has previously conducted an experiment without catalyst loading at 750 °C with an H_2O/AcOH ratio of 2.5. Results indicated only CO_2 and CH_4 formation, which suggested that decarboxylation of AcOH was the only reaction taking place in the absence of catalyst [35,37]. Results obtained in the presence of Ni@SiO_2 catalysts were summarized in Table 1. Results indicated the effect of temperature on both conversion and selectivity values. An increase in X_{AcOH} was observed with increasing temperature, as expected.

On the other hand, the impact of the H_2O/AcOH ratio on conversion was variant. This variant effect could be seen as a consecutive increase and decrease between H_2O/AcOH ratios of 2.5–5 and 5 to 7.5 ratios. This trend was only valid for 550 and 650 °C; at 750 °C, a gradual decrease of X_{AcOH} with increasing H_2O/AcOH ratios was observed, and this decrease was independent of Ni loading amount.

Statistical analyses revealed inconclusive results in the case of X_{AcOH} as the response, as expected, considering the ambiguous dependency of response (X_{AcOH}) on H_2O/AcOH ratio and Ni loading amount. On the other hand, meaningful results for S_{H2} responses were obtained and illustrated in Table 2.

Variance analysis for S_{H2} as the response resulted in the equation given below:

$$\text{Response } S_{H_2} = 53.6 + 0.036*A + 5.12*C - 3.39*B - 5.4E - 05*A*A - 0.229*C*C + 0.0284*B*B - 0.00543*A*C + 0.00467*A*B + 0.1425*C*B \quad (11)$$

Table 2 – Analysis of variance for S_{H2} response.

Model Summary

S	R-sq (%)	R-sq (adj,%)	PRESS	R-sq (pred,%)	MSE[a]	RMSE[a]	MAE[a]
1.88316	91.34	81.59	495.926	0.00%	0.0025	0.0498	1.078494

Source	DF	Seq SS	Adj SS	Adj MS	F	P	Cont. (%)
Model	9	299.158	299.158	33.24	9.37	<0.0001	91.34
Linear	3	221.022	218.139	72.713	20.5	<0.0001	67.48
A	1	133.225	128.866	128.866	36.34	**<0.0001**	**40.68**
B	1	87.405	88.685	88.685	25.01	**<0.0001**	**26.69**
C	1	0.392	0.588	0.588	0.17	0.695	0.12
Square	3	10.339	10.339	3.446	0.97	0.452	3.16
A[a]A	1	4.776	0.798	0.798	0.22	0.648	1.46
B[a]B	1	0.763	0.763	0.763	0.22	0.655	0.23
C[a]C	1	4.801	5.561	5.561	1.57	0.246	1.47
2 way interaction							
A[a]C	1	14.742	14.742	14.742	4.16	0.076	4.50
A[a]B	1	33.542	33.542	33.542	9.46	**0.015**	**10.24**
C[a]B	1	19.512	19.512	19.512	5.50	**0.047**	5.96
Error	8	28.370	28.370	3.546			**8.66**
Lack-of-fit	5	28.236	28.236	5.647	125.77	**0.001**	8.62
Pure error	3	0.135	0.135	0.045			
Total	17	327.538					**100**

[a] MSE, RMSE, and MAE corresponded to Mean squared error, root means squared error and mean absolute error, respectively.

The letters A, B, and C corresponded to temperature (°C), Ni loading amount (%), and H_2O/AcOH ratio, respectively. Response (S_{H2}) was shown with letter D (Fig. 1).

S_{H2} depended on temperature and Ni loading amount, as seen from Table 1. The effect of H_2O/AcOH ratio on S_{H2} could only be observed in the case of two-way interaction with temperature, and it should be noted that this effect was in the threshold with a p-value equal to 0.05 and results were evaluated as negligible for the effect of H_2O/AcOH on response. The impact of parameters was also illustrated as contour and three-dimensional response surface plots (Fig. 1 a and b). Results revealed selectivity values between 45 and 60% with two distinct zones of highest selectivity. S_{H2} was highest in the case of low temperatures and independent of Ni loading amount. At high temperatures, the highest S_{H2} values were obtained in the case of Ni loading amounts greater than 5% (Fig. 1 a and b).

Temperature values lower than 650 °C, indicated low X_{AcOH} values (Table 1). Evaluation of reaction experiments and statistical analyses showed that the highest X_{AcOH} and S_{H2} values could have been reached only at temperatures higher than 650 °C and preferably at Ni loading amounts between 5 and 10%. The change of reaction pattern with temperature was closely related to coke formation and hence elaborated in Coke formation and characterization of spent Ni@SiO2 catalysts Considering that the H_2O/AcOH ratio was ineffective on both conversion and selectivity, a H_2O/AcOH ratio of 2.5 would suffice in reaction experiments. Based on the

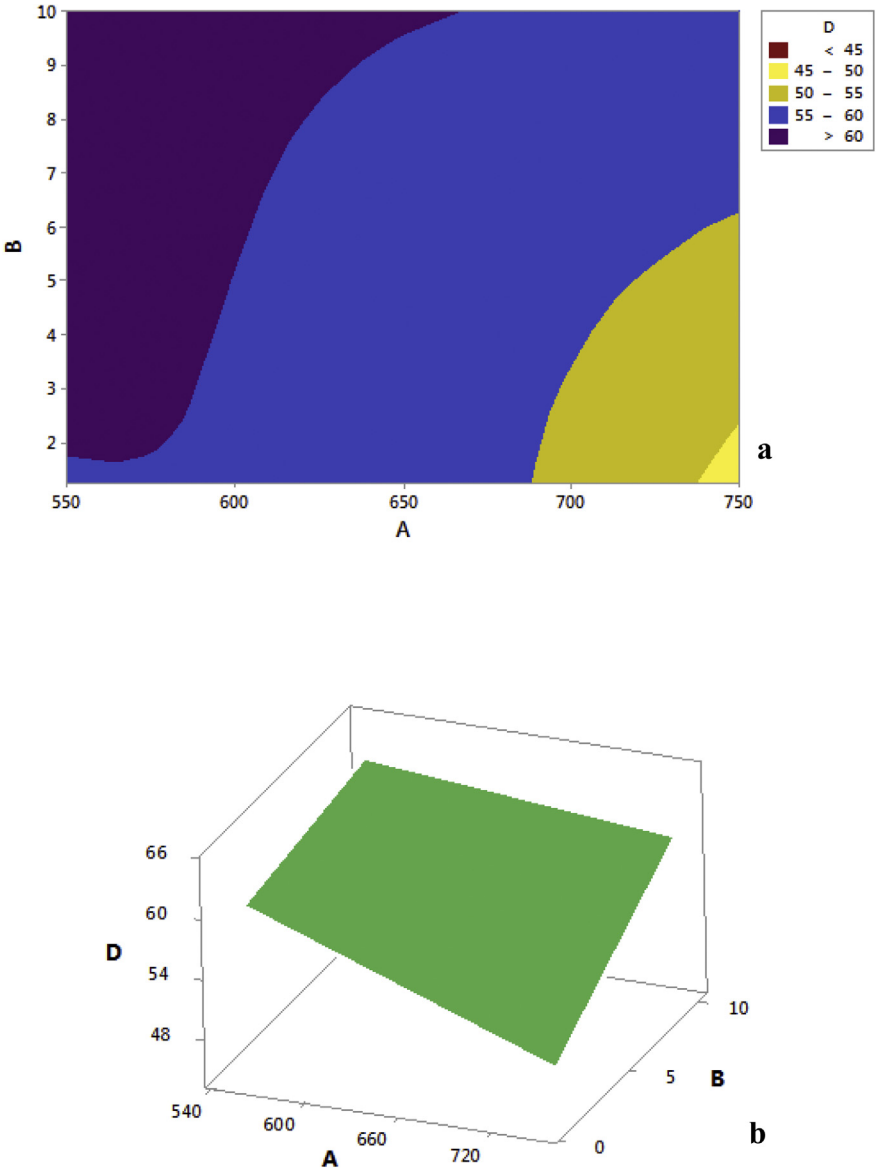

Fig. 1 – a) Contour and b) Response surface plots indicating the effect of parameters on S_{H2}.

results, catalysts involved in reactions at 750 °C with 1.25, 2.5, and 10% Ni loading were recovered and further investigated in characterization analyses.

Coke formation and characterization of spent Ni@SiO_2 catalysts

Reaction experiments were conducted for 3 h, and conversion values obtained at the end of 3 h were illustrated in Table 1. However, it would be best to give some examples of experimental results as a figure merely to indicate the effect of coke formation on catalytic activity (Fig. 2). The catalysts utilized in the experiments suffered from coke formation except for Ni@SiO_2 catalyst (10% Ni loading) used at 750 °C and with an H_2O/AcOH ratio of 2.5 (Fig. 2). The catalysts either used with a higher H_2O/AcOH ratio or temperatures below 750 °C indicated a severe loss of activity. Coke formation will eventually be observed regardless of the employed Ni amount, and it should be noted that the consistent activity trend observed with 10% Ni loading was simply due to reaction time. Nevertheless, this was one of the highlights of the study as given the right conditions (750/2.5; 10% loading), the catalytic activity could be preserved for at least 3 h of reaction.

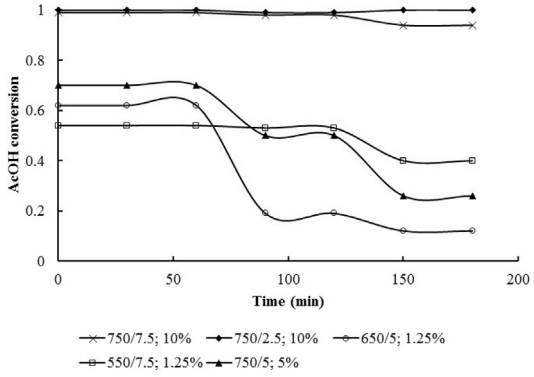

Fig. 2 – Selected AcOH conversions obtained from reaction experiments (See Table 1 for all results).

Coke formation could visually be detected from SEM images, as seen in Fig. 3. Fibrous and graphite were the most frequently determined coke formation. Fibrous coke was reported to have a less pronounced effect compared to graphite. Catalyst deactivation in the presence of graphite occurred as a result of active site blockage [13]. Graphite formation was validated by Raman spectroscopy with peaks obtained at 1337 and 1584 cm^{-1}. These peak values indicated the formation of D and G band of graphite, respectively (Fig. 4).

TGA analyses indicated two regions of weight loss. Initial weight loss ended approximately at 200 °C, emanated from the loss of water. The second region between 550 and 900 °C showed the removal of coke deposited on the catalyst surface. The highest coke amount was determined as 16% for the catalyst containing 10% Ni (Fig. 5). Ni presence in its metallic state was validated via XRD analysis of spent catalysts. The peak obtained at 26° belonged to graphite carbon and was visible for 10% Ni loading. Characterization results were in accordance, pointing out the formation of graphite, which appeared to be the main component responsible for activity decrease (Fig. 6). Crystal sizes calculated from Scherrer equation were 1.1, 2.2, and 4 nm for 1.25, 5, and 10% Ni loadings, respectively. Crystal growth below 5 nm indicated resistance of the catalyst to sintering [38].

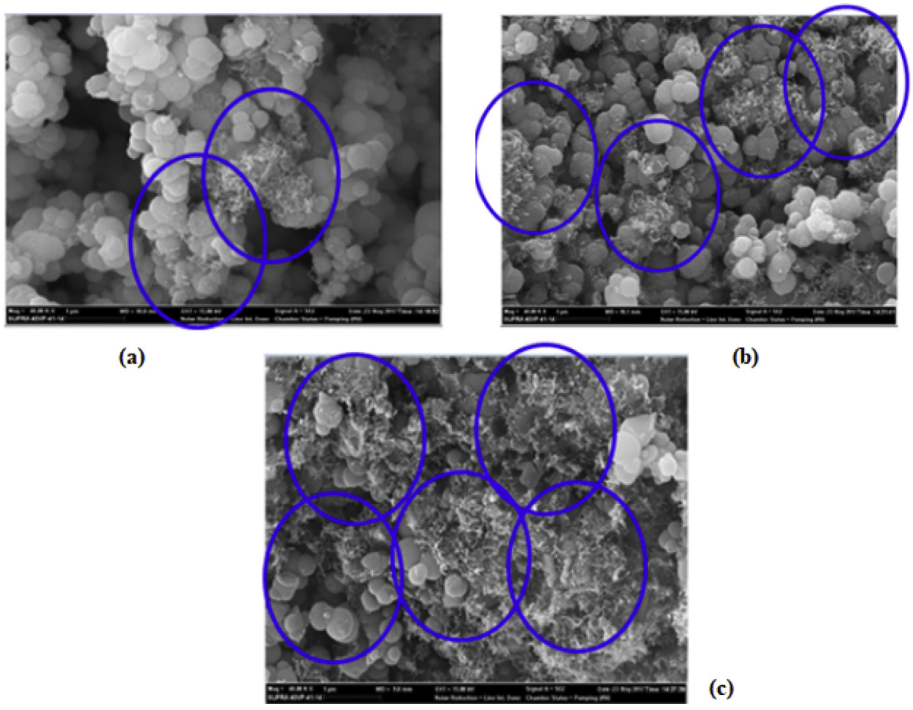

Fig. 3 – SEM images obtained from recovered catalysts utilized at 750 °C. Ni loading amounts: a) 1.25 b) 2.5 and c) 10%, respectively.

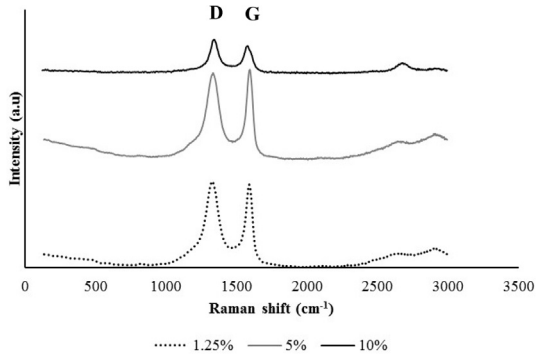

Fig. 4 – Raman spectroscopy analysis of spent catalysts recovered after reaction.

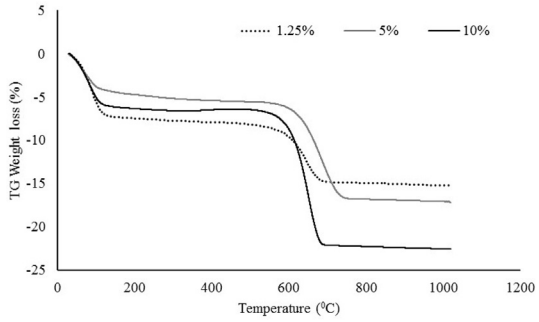

Fig. 5 – TGA analyses of spent catalysts recovered after the reaction.

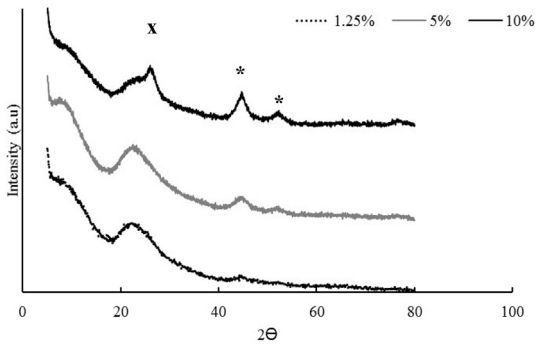

Fig. 6 – XRD patterns of spent catalysts recovered after the reaction. Graphite carbon was shown by "x," metallic nickel state was illustrated by "*" on the figure.

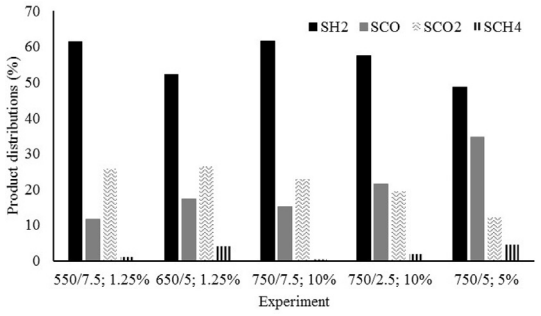

Fig. 7 – Product distributions obtained from selected experiments.

Acetic acid conversions were previously presented as an example to indicate the effect of coke on activity (Fig. 2). Product distributions obtained from these reaction experiments were also given to elaborate the sequence of reactions effective on catalyst activity and coke formation (Fig. 7). Steam reforming of acetic acid consisted of a complex network of reactions decreasing hydrogen selectivity. This decreasing effect became dominant, especially at high temperatures. Reaction experiments revealed the formation of CH_4, CO, CO_2, and H_2, along with a trace amount of acetone at high temperatures.

Particular emphasis on CO production should be given to understand the change of reaction pattern with temperature. An increase in the amount of CO produced with increasing temperature implied incomplete steam reforming due to a lack of active metal sites. This result also implied the necessity of increasing Ni loading in the catalyst structure. The opposite trend between CO_2 and CO selectivities with temperature increase could be explained by reverse water gas shift reaction (RWGS, $CO_2 + H_2 \leftrightarrow H_2O + CO$), increasing the amount of CO in the product stream. Boudouard reaction ($2CO \leftrightarrow C + CO_2$), leading to coke deposition, was also known to be effective at low temperatures [3,39]. Thus, the Boudouard reaction was unlikely to be among the sources of coke during the reaction at high temperatures. However, methane cracking ($CH_4 \leftrightarrow C + 2H_2$) becomes favorable at high temperatures.

As previously mentioned, hydrogen selectivities decreased with increasing temperature regardless of Ni loading amount (Fig. 1). This result implied the low possibility of methanation, which was known to be mitigated at temperatures higher than 625 °C [32]. Hence, decarboxylation of acetic acid was the only possible source of methane to lead coke formation. On the other hand, methane selectivities were obtained below 5% for all experiments, which implied a limited affinity of catalyst through decarboxylation reaction. Consequently, methane decomposition reaction could not be entirely responsible for coke deposition on catalyst structure.

The effect of the H_2O/AcOH ratio was statistically shown to be negligible on H_2 selectivities, and an ambiguous trend was obtained for AcOH conversions. In our opinion, the major effect of the H_2O/AcOH ratio was mitigating methanation reactions [36], which could be true considering a less pronounced decrease of activity at 750 °C compared to experiments conducted at 550 and 650 °C. Nevertheless, coke amounts reached to 16% (Fig. 5) indicated the presence of a coke source other than methane decomposition. As previously stated, a gradual decrease was observed for X_{AcOH} at 750 °C with an increasing H_2O/AcOH ratio. This decrease suggested the presence of ketonozation reaction [4]. Acetone was not present in product stream in any reaction, which implied the existence of a consecutive ketonozation and aldol-condensation reactions during the steam reforming of acetic acid. It was logical to assume the contribution of

acetone as a coke precursor considering high coke amounts obtained even at higher H_2O/AcOH ratios [3,4,14,36,40,41].

Suppressing carbon formation and maintaining high catalytic activity as combined tasks should be achieved for industrial applications. Hence catalytic activity and resistance to coke formation were adopted as two major goals in catalyst synthesis. Modifications in synthesis procedures that involve the joint addition of a second metal and a promoter were recently investigated to reach these goals [42–44]. Davidson et al. Investigated the effect of Co containing catalysts synthesized separately with the addition of $MgAl_2O_4$, ZnO, and CeO_2 used as promoters. Catalytic activity in steam reforming of acetic acid reached as high as 100 and 98% in terms of acetic acid conversion and H_2 selectivity. However, coke formation over 50% at the end of 4 h of reaction implied a decrease of activity in long-term utilization [42]. On the other hand, as stated in the work of Wang et al., a highest 9.6% coke deposition was detected for Ni–Fe/Palygosrkite catalysts modified with cerium [43], and coke deposition values for Rh supported on $La_2O_3/CeO_2–ZrO_2$ was only 2.95% in the work of Lemonidou et al. [44]. These catalysts indicated excellent results in terms of activity and stability. However, catalytic activity and stability could only be maintained by a combination of metals and promoters, increasing the synthesis costs.

Catalysts synthesized with only Ni utilization would beyond doubt decrease the start-up cost in industrial application. The catalysts utilized in the present study were compared with other Ni containing catalysts with two literature examples. These were given merely to provide an insight into the performance. Ni containing γ-Al_2O_3 catalysts with loading amounts greater than 15% reached 30% H_2 yield with 9% coke deposition in the work of An et al. [45]. The activity performance of Ni containing ZrO_2 catalysts was detected as 100 and >80% in terms of acetic acid conversion and H_2 selectivity in the work of Li. Et.al [39]. Coke deposition on the catalysts reached as high as 30% for the highest Ni loading [39]. Ni@SiO_2 microsphere catalysts in the present study were comparable with literature in terms of activity and coke deposition values. The catalytic activity of the catalyst with 10% Ni loading remained stable for 3 h even in the presence of 16% coke deposition. This result, considering the possibility of future works on modification of synthesis conditions and the components utilized in synthesis, implied the development of a catalyst compatible with industrial application.

Conclusions

Steam reforming of acetic acid in the presence of Ni@SiO_2 microsphere catalysts with varying Ni loading amounts was investigated with the present study. Effects of Ni loading amount, H_2O/AcOH ratio, and temperature on hydrogen selectivity and acetic acid conversions were determined via statistical analysis. Hydrogen selectivities were highest below 750 °C, which was the threshold for selectivity decrease. Product distributions obtained from a group of selected experiments revealed the impact of RWGS on the process and ruled out the possibility of Boudouard reaction as a coke source.

A statistical decrease of hydrogen selectivity with increasing temperature was attributed to the absence of methanation during the process. Methane decomposition was concluded to be inadequate in explaining coke formation during the steam reforming of acetic acid.

Based on reaction results and characterization studies, a noticeable decrease in activity due to graphite formation was observed. On the other hand, a stable activity for at least 3 h was validated with reaction experiments conducted at 750 °C (750/2.5; 1.25% Ni loading). This result was concluded to be among the highlights of the study, considering 16% coke formation during the reaction. Coke deposition, despite the adverse effect of H_2O/AcOH on methanation, implied the presence of a coke source other than methane. The gradual decrease in conversion values at 750 °C was interpreted as an indicator of ketonozation and aldol-condensation reactions, which consecutively occurred during the steam reforming of acetone.

Acknowledgments

The financial contribution of Bilecik Sheikh Edebali University Research Fund 2016-02. BŞEÜ.03–07 and contributions of Assistant Professor Dr. Yunus Emre Simsek are gratefully acknowledged.

Appendix A. Supplementary data

Supplementary data to this article can be found online at https://doi.org/10.1016/j.ijhydene.2020.05.146.

REFERENCES

[1] Calles JA, Carrero A, Vizcaino AJ, Megia PJ. Agglomerated CoeCr/SBA-15 catalysts for hydrogen production through acetic acid steam reforming. Int J Hydrogen Energy 2019;45(32):15941–50. https://doi.org/10.1016/j.ijhydene.2019.05.237.

[2] Dincer I, Acar C. Review and evaluation of hydrogen production methods for better sustainability. Int J Hydrogen Energy 2015;40(34):11094–111. https://doi.org/10.1016/j.ijhydene.2014.12.035.

[3] Borges RP, Ferreira RAR, Rabelo-Neto RC, Noronha FB, Hori CE. Hydrogen production by steam reforming of acetic acid using hydrotalcite type precursors. Int J Hydrogen Energy 2018;43:7881–92. https://doi.org/10.1016/j.ijhydene.2018.03.028.

[4] Phongprueksathat N, Meeyoo V, Rirksomboon T. Steam reforming of acetic acid for hydrogen production: catalytic performances of Ni and Co supported on $Ce_{0.75}Zr_{0.25}O_2$ catalysts. Int J Hydrogen Energy 2019;44:9359–67. https://doi.org/10.1016/j.ijhydene.2019.02.085.

[5] Zhang Z, Wang Y, Sun K, Shao Y, Zhang L, Zhang S, Zhang X, Liu Q, Chen Z, Hu X. Steam reforming of acetic acid over Ni-Ba/Al_2O_3 catalysts: impacts of barium addition on coking behaviors and formation of reaction intermediates. J Energy Chem 2020;43:208–19. https://doi.org/10.1016/j.jechem.2019.08.023.

[6] Hu X, Zhang L, Lu G. Pruning of the surface species on Ni/Al2O3 catalyst to selective production of hydrogen via acetone and acetic acid steam reforming. Appl Catal A-Gen. 2012;427–428:49–57. https://doi.org/10.1016/j.apcata.2012.03.029.

[7] Chen J, Wang M, Wang S, Li X. Hydrogen production via steam reforming of acetic acid over biochar-supported nickel catalysts. Int J Hydrogen Energy 2018;43:18160–8. https://doi.org/10.1016/j.ijhydene.2018.08.048.

[8] Li Z, Hu X, Zhang L, Liu S, Lu G. Steam reforming of acetic acid over Ni/ZrO_2 catalysts: effects of nickel loading and particle size on product distribution and coke formation. Appl Cata A-Gen. 2012;417–418:281–9. https://doi.org/10.1016/j.apcata.2012.01.002.

[9] Wang T, Ma H, Zeng L, Li D, Tian H, Xiao S. Highly loaded Ni-based catalysts for low-temperature ethanol steam reforming. Nanoscale 2016;8:10177–87. https://doi.org/10.1039/C6NR02586B.

[10] Lu M, Fang J, Han L, Faungnawakij K, Li H, Cai S, Shi L, Jiang H, Zhang D. Coke-resistant defect-confined Ni-based nanosheet-like catalysts derived from halloysites for CO2 reforming of methane. Nanoscale 2018;10:10528–37. https://doi.org/10.1039/C8NR02006J.

[11] Chenting Z, Hu X, Yu Z, Zhang Z, Chen G, Li C, Liu Q, Xiang J, Wang Y, Hu S. Steam reforming of acetic acid for hydrogen production over attapulgite and alumina supported Ni catalysts: impacts of properties of supports on catalytic behaviors. Int J Hydrogen Energy 2019;44:5230–44.

[12] Kumar A, Singh R, Sinha ASK. Catalyst modification strategies to enhance the catalyst activity and stability during steam reforming of acetic acid for hydrogen production. Int J Hydrogen Energy 2019;44:12983–3010. https://doi.org/10.1016/j.ijhydene.2019.03.136.

[13] Yu Z, Hu X, Jia P, Zhang Z, Dong D, Hu G, Hu S, Wang Y, Xiang J. Steam reforming of acetic acid over nickel-based catalysts: the intrinsic effects of nickel precursors on behaviors of nickel catalyst. Appl Catal B Environ 2018;237:538–53. https://doi.org/10.1016/j.apcatb.2018.06.020.

[14] Junior RBS, Rabelo-Neto RC, Gomes RS, Noronha FB, Frety R. Brandao ST Steam reforming of acetic acid over Ni-based catalysts derived from $La_{1-x}Ca_xNiO_3$ perovskite-type oxides. Fuel 2019;254:1–10. https://doi.org/10.1016/j.fuel.2019.115714.

[15] Pu J, Nishikago K, Wang N, Nguyen TT, Maki T, Qian EW. Core-shell nickel catalysts for the steam reforming of acetic acid. Appl Catal B Environ 2018;224:69–79. https://doi.org/10.1016/j.apcatb.2017.09.058.

[16] Basagiannis AC, Verykios XE. Catalytic steam reforming of acetic acid for hydrogen production. Int J Hydrogen Energy 2007;32:3343–55. https://doi.org/10.1016/j.ijhydene.2007.04.039.

[17] Sharma YC, Kumar A, Prasad R, Upadhyay SN. Ethanol steam reforming for hydrogen production: latest and effective catalyst modification strategies to minimize carbonaceous deactivation. Renew Sustain Energy Rev 2017;74:89–103. https://doi.org/10.1016/j.rser.2017.02.049.

[18] Pu J, Luo Y, Wang N, Bao H, Wang X, Qian EW. Ceria-promoted Ni@Al_2O_3 core-shell catalyst for steam reforming of acetic acid with enhanced activity and coke resistance. Int J Hydrogen Energy 2018;43:3142–53. https://doi.org/10.1016/j.ijhydene.2017.12.136.

[19] Bu K, Deng J, Zhang X, Kuboon S, Yan T, Li H, Shi L, Zhang D. Promotional effects of B-terminated defective edges of Ni/boron nitride catalysts for coking- and sintering-resistant dry reforming of methane. Appl Catal B Environ 2020;265:118692. https://doi.org/10.1016/j.apcatb.2020.118692.

[20] Bu K, Kuboon S, Deng J, Li H, Yan T, Chen G, Shi L, Zhang D. Methane dry reforming over boron nitride interface-confined and LDHs- derived Ni catalysts. Appl Catal B Environ 2019;252:86–97. https://doi.org/10.1016/j.apcatb.2019.04.007.

[21] Cao Y, Maitarad P, Gao M, Taketsugu T, Li H, Yan T, Shi L, Zhang D. Defect-induced efficient dry reforming of methane over two-dimensional Ni/h-boron nitride nanosheet catalysts. Appl Catal B Environ 2018;238:51–60. https://doi.org/10.1016/j.apcatb.2018.07.001.

[22] Liu C, Li S, Chen D, Xiao Y, Li T, Wang W. Hydrogen-rich syngas production by chemical looping steam reforming of acetic acid as bio-oil model compound over Fe-doped LaNiO3 oxygen carriers. Int J Hydrogen Energy 2019;44:17732–41. https://doi.org/10.1016/j.ijhydene.2019.05.148.

[23] Zhao X, Li H, Zhang J, Shi L, Zhang D. Design and synthesis of NiCe@m-SiO2 yolk-shell framework catalysts with improved coke-and sintering-resistance in dry reforming of methane. Int J Hydrogen Energy 2016;41:2447–56. https://doi.org/10.1016/j.ijhydene.2015.10.111.

[24] Majewski AJ, Wood J, Bujalski W. Nickel-silica core@shell catalyst for methane reforming. Int J Hydrogen Energy 2013;38:14531–41. https://doi.org/10.1016/j.ijhydene.2013.09.017.

[25] Yue L, Li J, Chen C, Fu X, Gong Y, Xia X, Hou j, Xiao C, Chen X, Zhao L, Ran G, Wang H. Thermal-stable Pd@mesoporous silica core-shell nanocatalysts for dry reforming of methane with good coke-resistant performance. Fuel 2018;218:335–41. https://doi.org/10.1016/j.fuel.2018.01.052.

[26] Wang F, Xu L, Shi W. Syngas production from CO_2 reforming with methane over core-shell Ni@SiO2 catalysts. J CO_2 Utilization 2016;16:318–27. https://doi.org/10.1016/j.jcou.2016.09.001.

[27] Zhao X, Xue Y, Yan C, Huang Y, Lu Z, Wang Z. Promoted activity of porous silica coated Ni/CeO_2ZrO_2 catalyst for steam reforming of acetic acid. Int J Hydrogen Energy 2017;42:21677–85. https://doi.org/10.1016/j.ijhydene.2017.07.086.

[28] Li L, Lu P, Yao Y, Ji W. Silica-encapsulated bimetallic Co-Ni nanoparticles as novel catalysts for partial oxidation of methane to syngas. Catal Commun 2012;26:72–7. https://doi.org/10.1016/j.catcom.2012.05.005.

[29] Das S, Ashok J, Bian Z, Dewangan N, Wai MH, Du Y, Borgna A, Hidajat K, Kawi S. Silica-Ceria sandwiched Ni core-shell catalyst for low-temperature dry reforming of biogas: coke resistance and mechanistic insights. Appl Catal B Environ 2018;230:220–36. https://doi.org/10.1016/j.apcatb.2018.02.041.

[30] Gunduz-Meric G, Arbag H, Degirmenci L. Coke minimization via SiC formation in dry reforming of methane conducted in the presence of Ni-based core–shell microsphere catalysts. Int J Hydrogen Energy 2017;42:16579–88. https://doi.org/10.1016/j.ijhydene.2017.05.121.

[31] Gunduz-Meric G, Degirmenci L. Validation of Consecutive Coke and SiC formation on Ni core-shell microspheres during methane decomposition. Catal Lett 2018;148:2127–32. https://doi.org/10.1007/s10562-018-2427-z.

[32] Gunduz-Meric G, Kaytakoglu S, Degirmenci L. Ni,Co/SiO_2 and Ni/SiO_2,Co bimetallic microsphere catalysts indicating high activity and stability in the dry reforming of methane. React Kinet Mech Catal 2020;129:403–19. https://doi.org/10.1007/s11144-019-01708-4.

[33] Gil MV, Fermoso J, Pevida C, Chen D, Rubiera F. Production of fuel-cell grade H2 by sorption enhanced steam reforming of acetic acid as a model compound of biomass-derived bio-oil. Appl Catal B:Environ 2016;184:64–76. https://doi.org/10.1016/j.apcatb.2015.11.028.

[34] Cakiryilmaz N, Arbag H, Oktar N, Dogu G, Dogu T. Effect of W incorporation on the product distribution in steam reforming of bio-oil derived acetic acid over Ni based Zr-SBA-15 catalyst. Int J Hydrogen Energy 2018;43:3629–42. https://doi.org/10.1016/j.ijhydene.2018.01.034.

[35] Cakiryilmaz N, Arbag H, Oktar N, Dogu G, Dogu T. Catalytic performances of Ni and Cu impregnated MCM-41 and Zr-MCM-41 for hydrogen production through steam reforming of acetic acid. Catal Today 2019;323:191–9. https://doi.org/10.1016/j.cattod.2018.06.004.

[36] Bossola F, Recchia S, Dal Sonto V. Catalytic steam reforming of acetic acid: latest advances in catalysts development and mechanism elucidation. Curr Catal 2018;7:89–98. https://doi.org/10.2174/2211544707666171219162653.

[37] Sahin Ozel S, Arbag H, Oktar N, Murtezaoglu K. Catalytic performances of Bi-metallic Ni-Co catalysts in acetic acid steam reforming reaction: effect of Mg incorporation. Int J Chem React Eng 2019;17(6). https://doi.org/10.1515/ijcre-2018-0164. 20180164, eISSN 1542-6580.

[38] Xin J, Cui H, Cheng Z, Zhou Z. Bimetallic Ni-Co/SBA-15 catalysts prepared by urea co-precipitation for dry reforming of methane. Appl Catal Gen 2018;554:95–104. https://doi.org/10.1016/j.apcata.2018.01.033.

[39] Li Z, Hu X, Zhang L, Liu S, Lu G. Steam reforming of acetic acid over Ni/ZrO2 catalysts: effects of nickel loading and particle size on product distribution and coke formation. Appl Catal Gen 2012;417–418:281–9. https://doi:10.1016/j.apcata.2012.01.002.

[40] Chen G, Tao J, Liu C, Yan B, Li W, Li X. Hydrogen production via acetic acid steam reforming: a critical review on catalysts. Renew Sustain Energy Rev 2017;79:1091–8. https://doi.org/10.1016/j.rser.2017.05.107.

[41] Pant KK, Mohanty P, Agarwal S, Dalai AK. Steam reforming of acetic acid for hydrogen production over bifunctional Ni-Co catalysts. Catal Today 2013;207:36–43. https://doi.org/10.1016/j.cattod.2012.06.021.

[42] Davidson SD, Spies KA, Mei D, Kovarik L, Kuntyakov I, Li XS, Dagle VL, Albrecht KO, Dagle RA. Steam reforming of acetic acid over Co-supported catalysts: coupling ketonization for greater stability. ACS Sustainable Chem Eng 2017;5:9136–49. https://doi.org/10.1021/acssuschemeng.7b02052.

[43] Wang Y, Chen M, Yang J, Liu S, Yang Z, Wang J, Liang T. Hydrogen production from steam reforming of acetic acid over Ni-Fe/palygorskite modified with cerium. BioResources 2017;12(3):4830–53. https://doi.org/10.15376/biores.12.3.4830-4853.

[44] Lemoniodu AA, Vagia EC, Lercher JA. Acetic acid reforming over Rh supported on La2O3/CeO2–ZrO2: catalytic performance and reaction pathway analysis. ACS Catal 2013;3:1919–28. https://doi.org/10.1021/cs4003063.

[45] An L, Dong C, Yang Y, Zhang J, He L. The influence of Ni loading on coke formation in steam reforming of acetic acid. Renew Energy 2011;36:930–5. https://doi.org/10.1016/j.renene.2010.08.029.